Chinese Chemical Letters 35 (2024) 108896

Contents lists available at ScienceDirect

Chinese Chemical Letters

journal homepage: www.elsevier.com/locate/cclet

Continuous-flow synthesis of polysubstituted γ-butyrolactones *via* enzymatic cascade catalysis

Liliang Chu[a,1], Xiaoyan Zhang[a,1], Jianing Li[a], Xuelei Deng[a], Miao Wu[b], Ya Cheng[b], Weiping Zhu[a], Xuhong Qian[a], Yunpeng Bai[a,*]

[a] State Key Laboratory of Bioreactor Engineering, Shanghai Collaborative Innovation Center for Biomanufacturing, East China University of Science and Technology, Shanghai 200237, China
[b] The Extreme Optoelectromechanics Laboratory, School of Physics and Materials Science, East China Normal University, Shanghai 200241, China

ARTICLE INFO

Article history:
Received 30 April 2023
Revised 30 July 2023
Accepted 3 August 2023
Available online 6 August 2023

Keywords:
Enzyme catalysis
Cascade catalysis
Directed evolution
Continuous-flow
γ-Butyrolactones

ABSTRACT

Polysubstituted chiral γ-butyrolactones are the core structural units of many natural products and high value-added flavors and fragrances used in the food and cosmetic industry. Current enzymatic cascade synthesis of these molecules faces the problems of low enzyme activity and phase separation in batch reaction, resulting in low productivity. Herein, we report a new continuous-flow process to synthesize the optically pure *Nicotiana tabacum* lactone (3*S*,4*S*)-**4a** and whisky lactone (3*R*,4*S*)-**4b** from α,β-unsaturated γ-ketoesters. A new ene reductase (ER) from *Swingsia samuiensis* (*Ss*ER) and a carbonyl reductase (*Ss*CR) were engineered by directed evolution to improve their activity and thermostability. The continuous-flow preparative reactions were performed in two 3D microfluidic reactors, generating (3*S*,4*S*)-**4a** (99% *ee* and 87% *de*) and (3*R*,4*S*)-**4b** (99% *ee* and 98% *de*) with space-time yields 3 and 7.4 times higher than those of the batch reactions. The significant enhancement in the productivity of enzyme cascade catalysis brought by cutting-edge continuous microfluidic technology will benefit the general multi-enzyme catalytic systems in the future.

Polysubstituted γ-butyrolactones are naturally occurring flavors and fragrances which are widely used in food, beverage, and cosmetics [1]. For example, 3,4-dimethyl substituted lactone, also known as *Nicotiana tabacum* lactone, exists in sun-cured tobacco leaves, featuring a pleasant herbaceous scent (Scheme 1) [2]. Whisky lactone is a flavor compound in alcoholic beverages that confers a typical coconut character [3]. In addition, many bioactive natural products and pharmaceuticals contain the core structures of polysubstituted γ-butyrolactones [4–10]. Hinokinin has displayed strong anti-inflammatory and antitrypanosomal activity [11–14]. Deoxyelephantopin can be used to treat hepatitis, arthritis, asthma, and cancer [5].

It is well known that the specific activity of these chiral compounds, *e.g.*, odor perception and bioactivity, is closely related to their stereo-configuration. Therefore, substantial effort has been devoted to the development of synthetic strategies for these α,β-disubstituted γ-butyrolactones. So far, carbene, transition metal, and organo-catalyzed reactions have been reported in the literature [15]. Typical examples include *N*-heterocyclic carbene catalyzed dynamic kinetic resolution of β-halo α-keto esters [16], a three-step Knoevenagl condensation-Michael addition-lactonization [17], and a sequential Michael-hemiacetalization-oxidation reaction based on organocatalysts [18].

Recently, Bobek *et al.* reported the total synthesis of polysubstituted γ-butyrolactone lignan derivatives through oxime carbonate cyclization from δ-nitro alcohols, delivering diverse γ-butyrolactones at ambient reaction conditions [19].

Alternatively, enzymatic pathways to these compounds have also attracted attention. Chiral γ-butyrolactones can be obtained by selective oxidation of racemic diols by alcohol dehydrogenase [20]. An impressive method uses enoate (or ene) reductases (ERs) to reduce the carbon-carbon double bond of α,β-unsaturated γ-ketoesters, followed by a stereoselective reduction of corresponding γ-ketoesters with carbonyl reductases (CRs). Classen *et al.* reported the cascade synthesis of β-methyl-substituted γ-valerolactone *via* this method [21], with an *ee* of 98%–99% and a maximum yield of 90%, but the product is limited to methyl-substituted short-chain lactones. Brenna *et al.* employed this route to synthesize **4a** with high stereoselectivity using Old Yellow Enzymes (OYEs, such as OYE1, OYE2, and OYE3 combined with al-

* Corresponding author.
E-mail address: ybai@ecust.edu.cn (Y. Bai).
[1] These authors contributed equally to this work.

https://doi.org/10.1016/j.cclet.2023.108896
1001-8417/

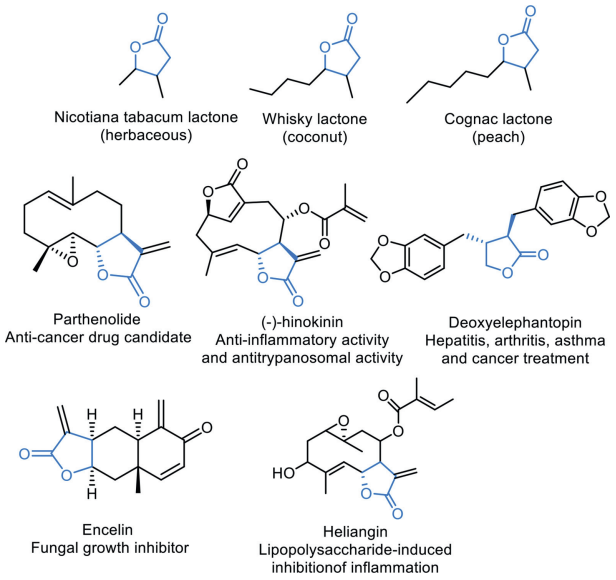

Scheme 1. Representative flavors, drugs, and bioactive natural products containing γ-butyrolactone-based structures.

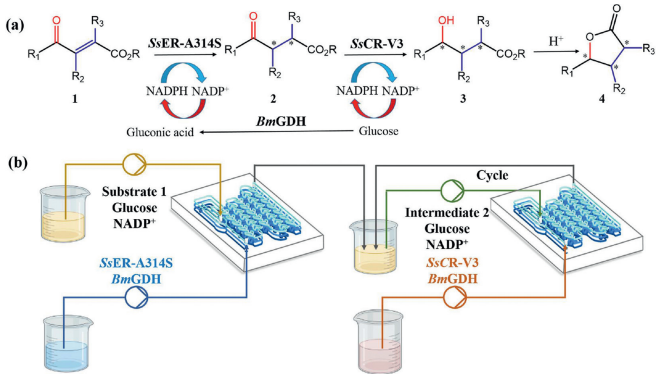

Scheme 2. Continuous-flow synthesis of chiral polysubstituted γ-butyrolactones *via* a dual-enzyme cascade catalysis.

cohol dehydrogenases [22]. Kumru *et al.* extended this method to prepare whisky and cognac lactones with moderate to good yields and very good diastereoselectivities [23].

Although the cascade enzymatic method has demonstrated its feasibility in the synthesis of polysubstituted γ-butyrolactones, the low activity of enzymes and phase separation in batch reaction led to low overall product yields and long reaction time. In particular, the second step of the cascade greatly limits the reaction time due to the imbalance in the activity of the two reactions (Scheme 2a). A key opportunity of multi-enzyme reactions in microreactors is the ability to perform *in vitro* biosynthetic reactions [24]. A number of continuous flow systems were used to overcome batch incompatibility by Mattey *et al.*, thus allowing for successful biocatalytic cascades [25]. Besides, Gruber *et al.* provide an overview of recent examples of cascaded microreactors [26]. Therefore, to address these issues, we presented a cascade continuous-flow approach for the synthesis of polysubstituted γ-butyrolactones in this study. We discovered a new ER, *Ss*ER from *Swingsia samuiensi*, through gene mining, and combined it with *Ss*CR (Protein Data Bank: 5GMO) [27]. Directed evolution of these two enzymes was performed to enhance their catalytic performance. In particular, we showed that the two reactions can be regulated in two 3D microfluidic reactors by controlling the flow rates of substrates and enzymes, significantly reducing the reaction time and enhancing the total reaction

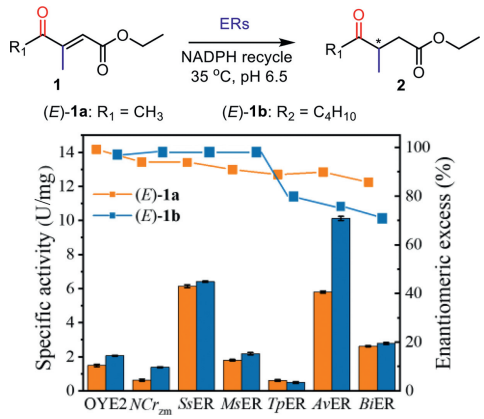

Fig. 1. Specific activity and stereoselectivity of ERs toward (*E*)–**1a** and (*E*)–**1b**.

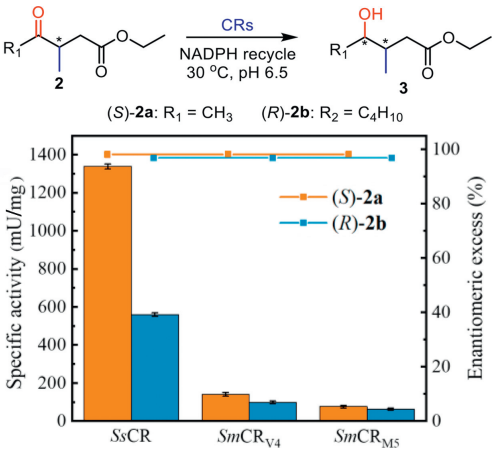

Fig. 2. Specific activity and stereoselectivity of CRs toward (*S*)–**2a** and (*R*)–**2b**.

efficiency (Scheme 2b). The detailed structures and sizes of the two microreactors are shown in Fig. S1 (Supporting information).

First, enzyme screening was performed with α,β-unsaturated γ-ketoesters (*E*)–**1a** and (*E*)–**1b** (Fig. 1). The protein sequences of OYE2 [22,28] and *NCr*$_{zm}$ [29] were used as the templates to carry out pBLAST searching in UniProt. A library of 13 gene sequences was obtained (sequence S1 in Supporting information), and 7 genes were expressed successfully into soluble recombinant enzymes in *Escherichia coli* (*E. Coli*) BL21 (DE3) (Table S1 and Fig. S2 in Supporting information). The specific activity and stereoselectivity of these ERs were assayed against (*E*)–**1a** and (*E*)–**1b** (Fig. 1 and Table S2 in Supporting information). Among them, *Ss*ER (from *Swingsia samuiensi*) displayed the highest activity of 6.1 U/mg and good (*S*)-stereoselectivity (93% *ee*) toward (*E*)–**1a**. *Ss*ER also exhibited higher activity than the templates OYE2 (1.5 U/mg) and *NCr*$_{zm}$ (0.6 U/mg) toward (*E*)–**1a**, and comparable stereoselectivity with OYE2 (98% *ee*) and *NCr*$_{zm}$ (93% *ee*). For (*E*)–**1b**, *Ss*ER showed higher activity (6.4 U/mg) and excellent (*R*)-stereoselectivity (99% *ee*) compared with OYE2 (2.1 U/mg, 98% *ee*) and *NCr*$_{zm}$ (1.4 U/mg, 99% *ee*). Thus, *Ss*ER was chosen for the first ene reduction in the following studies.

In addition, screening of the optimal CR with high conversion and enantioselectivity toward β-substituted γ-ketoesters was performed with (*S*)–**2a** and (*R*)–**2b** (Fig. 2). In previous studies, three CRs, including *Ss*CR, *Sm*CR$_{M5}$, and *Sm*CR$_{V4}$ have been demonstrated to show high activity and stereoselectivity toward γ-ketoacids and γ-ketoester without β-substituted groups [27,30,31]. In this assay, *Ss*CR (Fig. S3 in Supporting information) displayed the highest activity (1.3 and 0.6 U/mg) toward (*S*)–**2a** and (*R*)–**2b**, respectively.

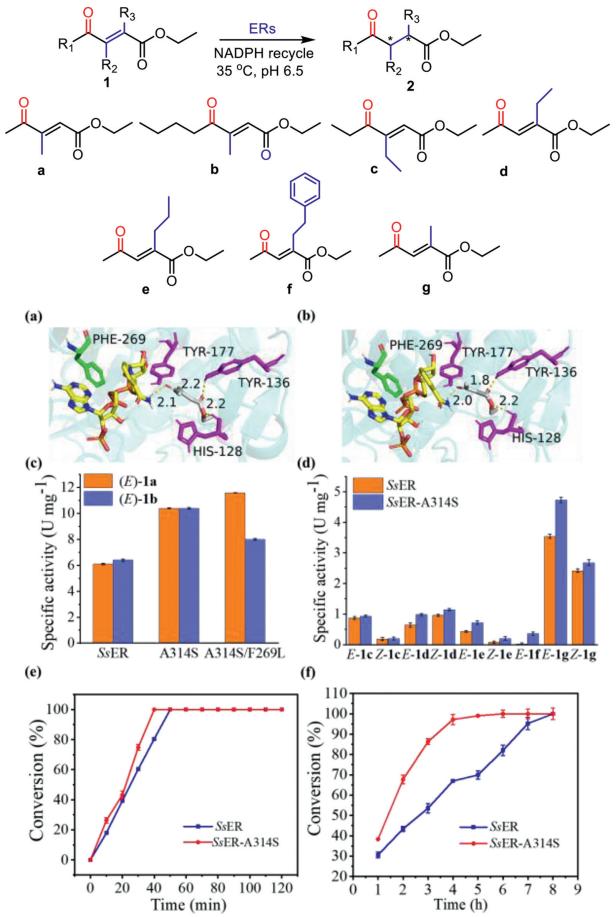

Fig. 3. Directed evolution of *Ss*ER. Molecular docking of (*E*)−**1a** into the active sites of *Ss*ER (a) and *Ss*ER-A314S (b). (c) The specific activity of *Ss*ER and variants toward (*E*)−**1a** and (*E*)−**1b**. (d) The specific activity of *Ss*ER and *Ss*ER-A314S toward different substrates. The time-course conversion of 8 mmol/L (*E*)−**1a** (e) and 8 mmol/L (*E*)−**1b** (f) by *Ss*ER and *Ss*ER-A314S. Conditions: (*E*)−**1a** and (*E*)−**1b** (8 mmol/L), $NADP^+$ (0.2 mmol/L), glucose (1.5 equiv.), lyophilized *Bm*GDH (10 mg), purified ERs (0.5 mg for (*E*)−**1a**) and 0.1 mg for ((*E*)−**1b**), 5% DMSO in 5 mL sodium phosphate buffer (100 mmol/L, pH 6.5), 35 °C.

The stereoselectivity was also excellent ((*S*)−99% *ee*). However, the activity of $SmCR_{M5}$ and $SmCR_{V4}$ toward these two substrates was much weaker (Tables S3 and S4 in Supporting information). Therefore, *Ss*CR was selected for further studies. The detailed preparation methods of the α,β-unsaturated γ-ketoesters can be found in the supporting information (Figs. S4 and S5 in Supporting information).

With the two enzymes in hand, we proceeded to construct an efficient synthetic route to polysubstituted γ-butyrolactones. To maximize the power of the continuous-flow chemistry, the catalytic performance of *Ss*ER and *Ss*CR needs further improvement via directed evolution. AlphaFold2 was used to build the three-dimensional protein structure models of *Ss*ER and its variants (https://alphafold.com/). (*E*)−**1a** was docked into the active pocket of *Ss*ER (Figs. 3a and b), and amino acid (a.a.) residues within 8 Å around the carbonyl oxygen of (*E*)−**1a** were selected for site-directed saturation mutation using NNK codons (Table S5 and sequence S2 in Supporting information).

Finally, variants *Ss*ER-A314S and A314S-F269L were obtained through plate screening. As shown in Table S6 (Supporting information), the specific activity of *Ss*ER-A314S-F269L toward (*E*)−**1a** and (*E*)−**1b** reached 11.6 and 8.0 U/mg, respectively. The specific activity of *Ss*ER-A314S toward (*E*)−**1a** and (*E*)−**1b** were enhanced to 10.4 U/mg (Fig. 3c). In addition, for (*E*)−**1a**, the kinetic analysis showed that the K_m of *Ss*ER-A314S did not change (15 μmol/L) compared with that of *Ss*ER, but the k_{cat} increased (Table S7, Figs. S6 and S7 in Supporting information). Therefore, the total catalytic efficiency of *Ss*ER-A314S (k_{cat}/K_m) is 1.4-fold higher than that of *Ss*ER. For (*E*)−**1b**, the K_m of *Ss*ER-A314S was reduced from 18 μmol/L to 5.7 μmol/L. Its k_{cat} was also increased, resulting in a 4.5-fold increase in the catalytic efficiency. Moreover, the activity of *Ss*ER-A314S toward a variety of substrates was all improved relative to *Ss*ER (Fig. 3d). *Ss*ER-A314S showed relatively high activity for α,β-saturated γ-ketoesters in the *E*-configuration, while it showed lower activity for the *Z*-configuration. Molecular docking of (*E*)−**1a** with SsER-A314S showed that the hydrogen bond distance formed between the ester group of the substrate and the Tyr136 residue of *Ss*ER was shortened from 2.2 Å to 1.8 Å after mutation (Figs. 3a and b). Therefore, the decreased distances involved in the hydride attack may contribute to the enhanced k_{cat}. In addition, the substrate was well stabilized during the reaction, which is also favorable for achieving smaller K_m. The total effect resulted in the enhanced catalytic efficiency of *Ss*ER-A314S.

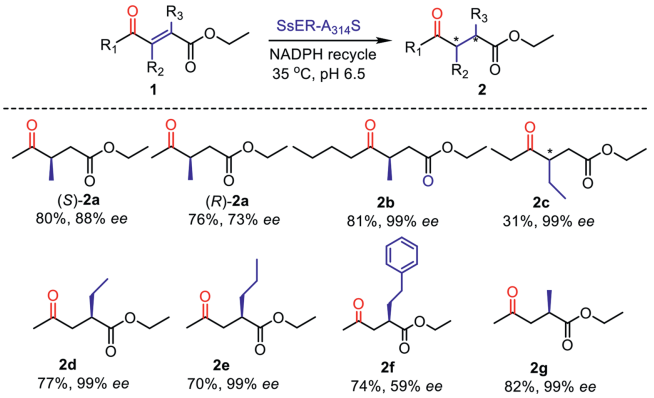

Fig. 4. Substrate scope. Chiral α- or β-substituted γ-ketoesters were synthesized by the variant *Ss*ER-A314S. Isolated yield and *ee* were determined by ^1H NMR and chiral GC. General procedure unless otherwise stated: **1a**-1g (50 mmol/L), 20 mL sodium phosphate buffer (pH 6.5, 100 mmol/L), $NADP^+$ (0.2 mmol/L), lyophilized *E. coli*/*Ss*ER-A314S (10 mg/mL), lyophilized *Bm*GDH (2 mg/mL) and glucose (75 mmol/L) at 35 °C for 12 h.

Subsequently, the time-course conversion of (*E*)−**1a** and (*E*)−**1b** catalyzed by *Ss*ER and *Ss*ER-A314S were determined, respectively. It can be seen that the rates of reactions catalyzed by *Ss*ER-A314S have been significantly improved compared with the wild type *Ss*ER (Figs. 3e and f). *Ss*ER-A314S achieved 100% conversion of 8 mmol/L (*E*)−**1a** and (*E*)−**1b** within 40 min and 6 h, respectively. Finally, we prepared a variety of α- and β-substituted chiral γ-ketoesters with *Ss*ER-A314S (Fig. 4). *Ss*ER-A314S showed good to excellent stereoselectivity (73%−99% *ee*) and high yield toward alkyl substituted α- and β-unsaturated γ-ketoesters ((*E*)−**1a**-(*E*)−1g)). In addition, *Ss*ER-A314S can also accept the α-aromatic substituted substrate (**3f**) and showed moderate enantioselectivity (59%) and isolated yield (74%). In addition, the half-lives of *Ss*ER-A314S were 577 h, 347 h, 90 h, and 39 min at 30 °C, 35 °C, 40 °C and 50 °C, respectively, which were up to 4-fold higher than those of *Ss*ER, indicating that the variant displayed improved thermostability (Fig. S8 in Supporting information).

Similarly, *Ss*CR was engineered to enhance its catalytic activity toward (*R*)−**2b** by engineering its active pocket (Figs. 5a and b, sequence S3 in Supporting information). First, the specific activity and k_{cat}/K_m of the variant *Ss*CR-V1 toward (*R*)−**2b** were 8.1 and 10 times higher than those of *Ss*CR, respectively (Tables S8 and S9, and Fig. S9 in Supporting information). However, it displayed a slight substrate inhibition. The second variant, *Ss*CR-V2, did not reduce substrate inhibition. According to a previous report [32], we

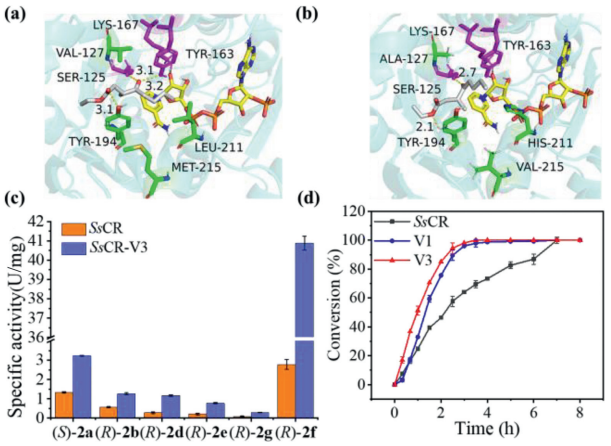

Fig. 5. Directed evolution of *Ss*CR. Molecular docking of (*R*)–**2b** into the active sites of *Ss*CR (**a**) and *Ss*CR-V3 (**b**). (**c**) The specific activity of *Ss*CR and V3 toward different substrates. (**d**) The time-course conversion of 20 mmol/L (*R*)–**2b** by *Ss*CR, V1, and V3. Reaction condition: (*R*)–**2b** (20 mmol/L), $NADP^+$ (0.2 mmol/L), Glucose (1.5 equiv.), lyophilized *Bm*GDH (10 mg), CRs (0.4 mg), 5% DMSO in 2 mL sodium phosphate buffer (100 mmol/L, pH 6.5), 30 °C.

introduced the mutation L211H into V2. The final variant V3 successfully eliminated the substrate inhibition and its specific activity against (*R*)–**2b** reached 1.3 U/mg. Moreover, the activity of *Ss*CR-V3 toward various substrates was enhanced compared with the wild-type *Ss*CR (Fig. 5c). In particular, V3 achieved 41 U/mg toward (*R*)–**2f**, which was 13.7-fold higher than that of *Ss*CR. Molecular docking of (*R*)–**2b** with *Ss*CR-V3 showed that the distance from the amino group of Ser125 to the carbonyl oxygen atom of the carboxyl group of the (*R*)–**2b** was shortened after mutation from 3.1 Å for *Ss*CR to 2.7 Å (Figs. 5a and b). Therefore, the decreased distances involved in the hydride attack and the proton transfer may contribute to enhancing catalytic efficiency. In addition, the half-lives of *Ss*CR-V3 were 238 and 36 h at 30 °C and 35 °C, respectively, which were enhanced 3.2- and 24-fold compared with those of *Ss*CR, indicating that the engineered enzyme had higher thermostability (Fig. S10 in Supporting information).

To further verify the improvement in catalytic performance, the conversion of (*R*)–**2b** by *Ss*CR and its variants (V1 and V3) was performed. The reaction rate was significantly enhanced after evolution. *Ss*CR-V3 reached 98% conversion within 3 h, while *Ss*CR converted only 64% (*R*)–**2b** at the same time (Fig. 5d). These results indicated that V3 was suitable for the asymmetric reduction of γ-ketoesters.

With *Ss*ER-A314S and *Ss*CR-V3 in hand, we performed a one-pot two-step sequential reaction to synthesize *Nicotiana tabacum* lactone ((3*S*,4*S*)–**4a**) and whisky lactone ((3*R*,4*S*)–**4b**) in a preparative scale (Table 1). For (3*S*,4*S*)–**4a**, the first ene reduction took 6 h to reach substrate conversion >99%, and then *Ss*CR-V3 was added into the reaction to achieve 90% conversion within 20 h. The total reaction time was 26 h, generating (3*S*,4*S*)–**4a** at 56% yield with excellent optical purity (99% *ee*) and good diastereoselectivity (87% *de*). For (3*R*,4*S*)–**4b**, *Ss*ER-A314S also converted the substrate (*E*)–**1a** >99% within 6 h in the first step, however, *Ss*CR-V3 catalyzed the carbonyl reduction even slower, reaching 87% conversion with 99% *ee* and 98% *de* after 36 h. The total reaction time reached 42 h and the final yield was 53%.

These results showed that the second carbonyl reduction is the rate-limiting step, which is consistent with the previous report [23]. However, the two steps cannot be combined in a single-step one-pot reaction because *Ss*CR-V3 can also catalyzes the α,β-unsaturated γ-ketoesters, generating allylic alcohols which are not accepted by *Ss*ER-A314S. Furthermore, the reaction's high substrate

Table 1
One-pot synthesis of optically pure γ-butyrolactones.[a]

Product	Time (h)	Conv. (%)	Yield (%)[c]	*ee* (%)	*de* (%)
 (3*S*,4*S*)–**4a**	26	90	56	99	87
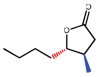 (3*R*,4*S*)–**4b**	42[b]	87	53	99	98

[a] Reaction conditions: substrate (50 mmol/L), glucose (75 mmol/L), $NADP^+$ (0.2 mmol/L), lyophilized *E. coli*/*Ss*ER-A314S (10 g/L), lyophilized *E. coli*/*Bm*GDH (2 g/L), lyophilized *E. coli*/*Ss*CR-V3 (10 g/L), sodium phosphate buffer (pH 6.5, 100 mmol/L), 35 °C.
[b] Purified *Ss*CR-V3 (15 U) instead of lyophilized *E. coli*/*Ss*CR-V3 (10 g/L).
[c] The isolated yield was determined by GC.

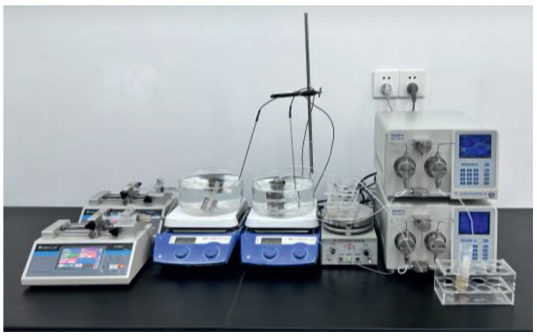

Fig. 6. Continuous-flow synthesis of chiral polysubstituted γ-butyrolactones *via* a dual-enzyme cascade.

loading (50 mmol/L) was essential for obtaining scaled-up preparation. However, phase separation was observed because of the low substrate solubility in water, which also limited the overall reaction rate.

The continuous-flow process carried out automatically in a microreactor can improve biocatalysis performance, making large-scale bioproduction more cost-effective due to significantly reduced reaction volume, improved mass transfer, shorter reaction time, and improved space-time yield [33]. To further increase the overall reaction rate, we performed the preparative reaction in two 3D microfluidic reactors in a continuous-flow manner (Fig. 6). In the first microfluidic reactor, the double bond reduction proceeded with >99% conversion in 30 min, thanks to the solved substrate (5 mmol/L) and the high enzyme activity of *Ss*ER-A314S. Then, the intermediate α,β-substituted γ-ketoesters were injected into the second microreactor together with *Ss*CR-V3 and converted into the final products. Considering the relatively lower activity of *Ss*CR-V3, the second reaction was cycled a couple of times to improve the total conversion. As expected, the second reaction took 26 min to reach 93% conversion for (3*S*,4*S*)–**4a** with the same stereoselectivity (99% *ee* and 87% *de*). The total reaction time was reduced to 56 min (Table 2), and the space-time yield reached approximately 5.0 mmol L^{-1} h^{-1}, which was 3 times higher than that of the batch reaction (1.7 mmol L^{-1} h^{-1}). For (3*R*,4*S*)–**4b**, the total reaction time was reduced to 40 min without any appreciable loss of optical purity, giving a space-time yield of 7.4 mmol L^{-1} h^{-1} which was 7.4 times higher than that of the batch reaction (1.0 mmol L^{-1} h^{-1}). The reduction in reaction time can be attributed to the elimination of phase separation and enhanced mixing of reactants in the 3D microfluidic reactors. Although the continuous-flow was run at a low substrate concentration, the automatic operation and independent control over the flow rates allow for the parallel syn-

Table 2
Continuous-flow synthesis of γ-butyrolactones.[a]

Product	Time (min)	Conv. (%)	Yield (%)[b]	*ee* (%)	*de* (%)
 (3*S*,4*S*)–**4a**	56	93	93	99	87
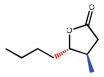 (3*R*,4*S*)–**4b**	40	99	99	99	98

[a] Reaction conditions: (*E*)–**1a** or (*E*)–**1b** (5 mmol/L), glucose (1.5 equiv.), $NADP^+$ (0.2 mmol/L), lyophilized *E. coli*/*Ss*ER-A314S (10 U/mL), lyophilized *E. coli*/*Bm*GDH (15 U/mL), lyophilized *E. coli*/*Ss*CR-V3 (10 U/mL), sodium phosphate buffer (pH 6.5, 100 mmol/L), 35 °C.
[b] The analytical yield was determined by GC.

thesis of γ-butyrolactones. In particular, future improvements in enzyme catalytic activity will further enhance the productivity of the continuous-flow process, while the batch reaction benefits little from this because the serious phase separation remains at high substrate loading.

In conclusion, the improvement of efficiency and productivity of cascade enzymatic processes relies on the combination of biocatalyst engineering and process optimization. Herein, we engineered an ene reductase *Ss*ER and a carbonyl reductase *Ss*CR, which displayed improved activity and thermostability compared with the wild-type enzymes. We proved that the optically pure *Nicotiana tabacum* lactone ((3*S*,4*S*)–**4a**) and whisky lactone ((3*R*,4*S*)–**4b**) can be synthesized efficiently from α,β-unsaturated ketoesters in the continuous-flow process, delivering products with 3 and 7.4 times higher space-time yields compared with the one-pot, two-step batch reaction. The integration of cascade enzyme catalysis into cutting-edge continuous microfluidic technology will benefit the general *in vitro* multi-enzyme catalytic systems in the future.

Declaration of competing interest

The authors declare that they have no known competitive financial interests or personal relationships that may affect the work of this report.

Acknowledgments

This work was financially sponsored by the National Key Research and Development Program of China (No. 2021YFC2102804) and the National Natural Science Foundation of China (No. 22078096).

Supplementary materials

Supplementary material associated with this article can be found, in the online version, at doi:10.1016/j.cclet.2023.108896.

References

[1] A. Świzdor, A. Panek, N. Milecka-Tronina, et al., Int. J. Mol. Sci. 13 (2012) 16514–16543.
[2] B. Kimland, J. Aasen, S.O.A. lmqvist, P. Arpino, C.R. Enzell, Phytochemistry 12 (1973) 835–847.
[3] E. Masson, R. Baumes, C.L. Guernev, J.L. Puech, J. Agric, Food Chem. 48 (2000) 4306–4309.
[4] V.B. Mathema, Y.S. Koh, B.C. Thakuri, M. Sillanpää, Inflammation 35 (2012) 560–565.
[5] F.A. Kabeer, R. Prathapan, Pharmacologia 5 (2014) 272–285.
[6] A.A. Beeran, N. Maliyakkal, M.C. Rao, N. Udupa, Pharmacogn. Mag. 11 (2015) 257–268.
[7] C. Li, H. Wu, Y. Yang, J. Liu, Z. Chen, Oncol. Lett. 15 (2018) 9673–9680.
[8] C.L. Li, H.Z. Wu, Y.P. Huang, et al., Pharmacotherapy 6 (2008) 401–409.
[9] M. Sabanero, L. Quijano, T. Rios, R. Trejo, Planta Med. 61 (1995) 185–186.
[10] X.G. Lu, M. L, J.L. Wei, et al., Biomed. Pharmacother. 88 (2017) 102–108.
[11] R.D. Silva, G.H.B.D. Souza, A.A.D. Silva, et al., Bioorg. Med. Chem. Lett. 15 (2005) 1033–1037.
[12] T.C. Lima, R. Lucarini, A.C. Volpe, et al., Med. Chem. Lett. 27 (2017) 176–179.
[13] V.A.D. Souza, R.D. Silva, A.C. Pereira, et al., Bioorg. Med. Chem. Lett. 15 (2005) 303–307.
[14] J. Saraiva, C. Vega, M. Rolon, et al., Parasitol. Res. 100 (2007) 791–795.
[15] J. Hur, J. Jang, J. Sim, Int. J. Mol. Sci. 22 (2021) 2769.
[16] C.G. Goodman, M.M. Walker, J.S. Johnson, J. Am. Chem. Soc. 137 (2015) 122–125.
[17] T.M. Khopade, A.D. Sonawane, J.S. Arora, R.G. Bhat, Adv. Synth. Catal. 35 (2017) 3905–3910.
[18] P. Mahto, N.K. Rana, K. Shukla, et al., Org. Lett. 21 (2019) 5962–5966.
[19] K.B. Bobek, N.S. Ezzat, B.S. Jones, et al., Org. Lett. 25 (2023) 31–36.
[20] F. Boratyński, K. Dancewicz, M. Paprocka, B. Gabryś, C. Wawrzeńczyk, PLoS One 11 (2016) e0146160.
[21] T. Classen, M. Korpak, M. Schölzel, J. Pietruszka, ACS Catal. 4 (2014) 1321–1331.
[22] E. Brenna, F.G. Gatti, D. Monti, et al., J. Mol. Catal. B 114 (2015) 77–85.
[23] C. Kumru, T. Classen, J. Pietruszka, ChemCatChem 10 (2018) 4917–4926.
[24] M.Y. Lee, A. Srinivasan, B. Ku, J.S. Dordick, Biotechnol. Bioeng. 83 (2003) 20–28.
[25] A.P. Mattey, G.J. Ford, J. Citoler, Angew. Chem. Int. Ed. 60 (2021) 18660–18665.
[26] P. Gruber, M.P.C. Marques, B. O'Sullivan, et al., Biotechnol. J. 12 (2017) 1700030.
[27] Y.Q. Zhang, T.T. Feng, Y.F. Cao, et al., ACS Catal. 11 (2021) 10487–10493.
[28] A. Goffeau, B.G. Barrell, H. Bussey, et al., Science 274 (1996) 546–567.
[29] M. Hall, C. Stueckler, B. Hauer, et al., Eur. J. Org. Chem. 2008 (2008) 1511–1516.
[30] T. Wang, X.Y. Zhang, Y.C. Zheng, Y.P. Bai, Chem. Commun. 57 (2021) 10584–10587.
[31] M. Chen, X.Y. Zhang, C.G. Xing, et al., ChemCatChem 11 (2019) 2600.
[32] Y.P. Shang, Qi. Chen, A.T. Li, et al., J. Biotech. 308 (2020) 141–147.
[33] Y. Wu, W.Q. Chen, Y.Q. Zhao, et al., Chin. Chem. Lett. 26 (2015) 334–338.